Research Article Vol. 38, No. 3 / March 2021 / Journal of the Optical Society of America A 405

Journal of the Optical Society of America A

OPTICS, IMAGE SCIENCE, AND VISION

Solutions for single-scattered radiance in the semi-infinite medium based on radiative transport theory

André Liemert,* Simeon Geiger, and Alwin Kienle

Institut für Lasertechnologien in der Medizin und Meßtechnik, Helmholtzstr. 12, D-89081 Ulm, Germany
**Corresponding author: andre.liemert@ilm-ulm.de*

Received 10 September 2020; revised 20 January 2021; accepted 26 January 2021; posted 27 January 2021 (Doc. ID 409898); published 19 February 2021

In this paper, some explicit analytical solutions for single-scattered radiance in a half-space medium under consideration of a reflecting boundary are derived. We consider both a unidirectional beam source as well as an isotropic point source. In addition to direct applications within optical tomography and computer graphics, the obtained solutions are also needed when solving the radiative transport equation after the separation of the unscattered and single-scattered contribution. Comparisons between the derived analytical solutions and the Monte Carlo method display excellent agreement.

https://doi.org/10.1364/JOSAA.409898

1. INTRODUCTION

The radiative transport equation (RTE) is a pivotal equation involved in many areas of science such as astrophysics, neutron transport, climate research, heat transfer, and biomedical optics [1–3]. Another area of application, where solutions of the RTE are needed, is the computer graphics field, in particular, physically based rendering [4–9]. For prediction of the light propagation in random media, the RTE provides in many situations a valid approximation of Maxwell's equations [10], avoiding the high computational cost needed to solve Maxwell's equations. Within the medical physics field, the RTE is often applied in the context of fluorescence spectroscopy, quantitative microscopy, bioluminescence imaging, or photodynamic therapy [11]. Due to the complexity of the RTE, different approximations to this equation were applied to derive analytical solutions. The best known approximation, which is still widely used, is the diffusion equation. For example, diffusion-based models under consideration of extrapolated boundary conditions have been used for rendering translucent semi-infinite materials [5]. However, it is well known that the diffusion approximation cannot be used within several situations of high practical importance, especially if one is interested in solutions after one or two scattering events. Concerning numerical methods, the Monte Carlo simulation is the most often used approach to solve the RTE [12]. Apart from this, other numerical schemes concerning the RTE have been developed such as the finite difference method, the finite element approach, or the finite volume method. For more details, we refer to other publications [13–15]. The numerical methods have the advantage that they are less restricted concerning the considered geometry, but they usually are approximated and slower compared to the analytical solutions. In this context, it should also be mentioned that analytical solutions are quite useful to verify the different numerical schemes. In recent years, several analytical approaches, such as the method of rotated reference frames [16–18] or the singular eigenfunction method [19], have been developed to solve the RTE. In addition, some explicit analytical solutions of the RTE in the P_3 approximation have been derived in [20]. Apart from this, analytical solutions in the P_1 approximation have been reported in [21–23], and single-scattering solutions of the time-dependent RTE have been considered in [24,25]. The solutions presented in our earlier work [17] are based on the modified spherical harmonics method, which involves the numerical determination of eigenvalues. Further, for evaluation of the angular radiance, many terms of the spherical harmonics series must be taken into account. In the present case of single-scattered radiance, there is the possibility to derive a closed-form expression for radiance in terms of elementary functions. As mentioned above, RTE solutions are also used for physically based rendering applications. In particular, single-scattering RTE solutions expressed in terms of the so-called air–light integral have been derived for infinitely extended turbid media and successfully applied in recent years [26,27].

In this paper, we derive new explicit analytical solutions for the single-scattered radiance within the infinite and semi-infinite medium considering the exact reflecting boundary condition via Fresnel's equations. In addition to the unidirectional beam source with an arbitrary direction, we also consider the important case of an isotropic point source. All solutions

are general in view of the boundary reflection function and the scattering phase function. The derived analytical solutions are applicable within optical tomography and computer graphics, and to solve the RTE after separation of the unscattered and the single-scattered contribution.

2. SINGLE-SCATTERED RADIANCE DUE TO A UNIDIRECTIONAL POINT SOURCE

In this section, we derive an analytical solution for single-scattered radiance I_1 due to a unidirectional δ source located in the half-space $V = \{\mathbf{x} \in \mathbb{R}^3 | z > 0\}$ and radiating along an arbitrary direction $\mathbf{\Omega}_0$. For this task, we first must consider the unscattered component I_0 obeying

$$\begin{aligned}\mathbf{\Omega} \cdot \nabla I_0(\mathbf{x}, \mathbf{\Omega}) + \sigma_t I_0(\mathbf{x}, \mathbf{\Omega}) \\ = \delta(\mathbf{x} - \mathbf{x}_0)\delta(\mathbf{\Omega} - \mathbf{\Omega}_0) \\ + R(-\mu_0)\Theta(-\mu_0)\delta(\mathbf{x} + \mathbf{x}_0)\delta(\mathbf{\Omega} - \mathbf{\Omega}_{0'}),\end{aligned} \tag{1}$$

where $(\mathbf{x}, \mathbf{\Omega}) \in \overline{V} \times \mathbb{S}^2$, $\mathbf{x}_0 = (0, 0, z_0) \in V$, R is the reflection function (e.g., obtained from Fresnel's equations), $\mathbf{\Omega}'_0 = \mathbf{\Omega}(-\mu_0, \phi_0)$, and Θ denotes the step function. The unit vector $\mathbf{\Omega}$ specifying the direction is defined as

$$\mathbf{\Omega} = \begin{pmatrix} \sin\theta\cos\phi \\ \sin\theta\sin\phi \\ \cos\theta \end{pmatrix} = \begin{pmatrix} \sqrt{1-\mu^2}\cos\phi \\ \sqrt{1-\mu^2}\sin\phi \\ \mu \end{pmatrix} =: \mathbf{\Omega}(\mu, \phi). \tag{2}$$

Furthermore, we have $\sigma_t = \sigma_a + \sigma_s$ as the total attenuation coefficient with σ_a and σ_s as the absorption and scattering coefficient, respectively. The right-hand side of Eq. (1) depends on the direction of the unidirectional point source. In the case of $\mu_0 > 0$, only one source is present; for $\mu_0 < 0$, however, an additional image source is taken into account to incorporate the reflection of the beam at the boundary. As a result, the particular solution of Eq. (1) will directly satisfy the intended boundary condition

$$I_0(\mathbf{x}, \mu, \phi) = R(\mu) I_0(\mathbf{x}, -\mu, \phi), \quad (\mathbf{x}, \mu) \in \partial V \times (0, 1]. \tag{3}$$

For illustration purposes, Fig. 1 schematically shows the geometry of the problem, including the source configuration to define the scattering and reflecting half-space.

Using the unscattered radiance [1] that satisfies $(\partial_{\mathbf{\Omega}} + \sigma_t)(\cdot) = \delta(\mathbf{x} - \mathbf{x}_0)\delta(\mathbf{\Omega} - \mathbf{\Omega}_0)$, the solution of Eq. (1) can be written as

$$\begin{aligned}I_0(\mathbf{x}, \mathbf{\Omega}) = \frac{\exp(-\sigma_t \| \mathbf{x} - \mathbf{x}_0 \|)}{\| \mathbf{x} - \mathbf{x}_0 \|^2} \delta\left(\frac{\mathbf{x} - \mathbf{x}_0}{\| \mathbf{x} - \mathbf{x}_0 \|} - \mathbf{\Omega}_0 \right) \delta(\mathbf{\Omega} - \mathbf{\Omega}_0) \\ + R(-\mu_0)\Theta(-\mu_0) \frac{\exp(-\sigma_t \| \mathbf{x} + \mathbf{x}_0 \|)}{\| \mathbf{x} + \mathbf{x}_0 \|^2} \\ \times \delta\left(\frac{\mathbf{x} + \mathbf{x}_0}{\| \mathbf{x} + \mathbf{x}_0 \|} - \mathbf{\Omega}'_0 \right) \delta(\mathbf{\Omega} - \mathbf{\Omega}'_0).\end{aligned} \tag{4}$$

The single-scattered radiance is defined as a solution of

$$\mathbf{\Omega} \cdot \nabla I_1(\mathbf{x}, \mathbf{\Omega}) + \sigma_t I_1(\mathbf{x}, \mathbf{\Omega}) = S_1(\mathbf{x}, \mathbf{\Omega}), \tag{5}$$

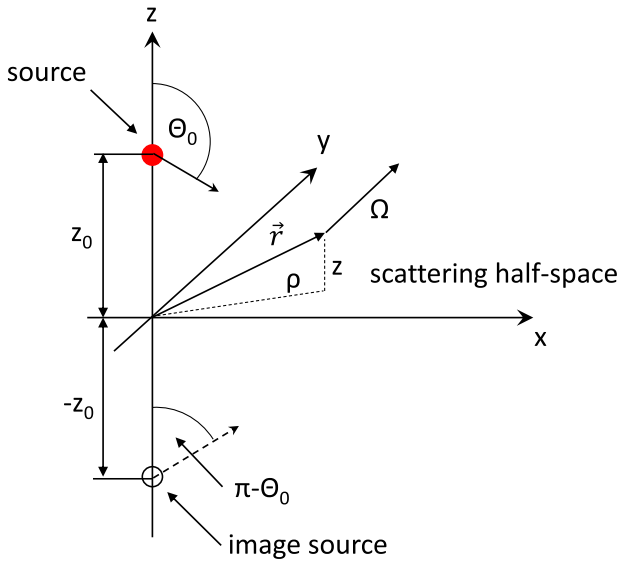

Fig. 1. Illustration of the half-space geometry, including the position and direction of the two unidirectional point sources.

where $S_1(\mathbf{x}, \mathbf{\Omega}) = \sigma_s \int f(\mathbf{\Omega} \cdot \mathbf{\Omega}') I_0(\mathbf{x}, \mathbf{\Omega}') \mathrm{d}\mathbf{\Omega}'$ is the corresponding source term that is given by

$$\begin{aligned}S_1(\mathbf{x}, \mathbf{\Omega}) = \sigma_s \frac{\exp(-\sigma_t \| \mathbf{x} - \mathbf{x}_0 \|)}{\| \mathbf{x} - \mathbf{x}_0 \|^2} \delta\left(\frac{\mathbf{x} - \mathbf{x}_0}{\| \mathbf{x} - \mathbf{x}_0 \|} - \mathbf{\Omega}_0 \right) f(\mathbf{\Omega} \cdot \mathbf{\Omega}_0) \\ + \sigma_s R(-\mu_0)\Theta(-\mu_0) \frac{\exp(-\sigma_t \| \mathbf{x} + \mathbf{x}_0 \|)}{\| \mathbf{x} + \mathbf{x}_0 \|^2} \\ \times \delta\left(\frac{\mathbf{x} + \mathbf{x}_0}{\| \mathbf{x} + \mathbf{x}_0 \|} - \mathbf{\Omega}'_0 \right) f(\mathbf{\Omega} \cdot \mathbf{\Omega}'_0),\end{aligned} \tag{6}$$

with $f : [-1, 1] \to \mathbb{R}_0^+$ being the normalized scattering phase function. The associated boundary condition (BC) for the single-scattered radiance is the same as that for the unscattered part given in Eq. (3). The particular solution of Eq. (5), which will be denoted by G_1, is formally given by

$$G_1(\mathbf{x}, \mathbf{\Omega}) = \int_0^\infty S_1(\mathbf{x} - \ell\mathbf{\Omega}, \mathbf{\Omega}) \exp(-\sigma_t \ell) \mathrm{d}\ell, \tag{7}$$

with S_1 from Eq. (6). In this context, it will be useful to introduce the quantity

$$\begin{aligned}U(\mathbf{x}, \mathbf{\Omega}, \mathbf{\Omega}_0) := \int_0^\infty \exp(-\sigma_t \ell) \frac{\exp(-\sigma_t \| \mathbf{x} - \ell\mathbf{\Omega} \|)}{\| \mathbf{x} - \ell\mathbf{\Omega} \|^2} \\ \times \delta\left(\frac{\mathbf{x} - \ell\mathbf{\Omega}}{\| \mathbf{x} - \ell\mathbf{\Omega} \|} - \mathbf{\Omega}_0 \right) \mathrm{d}\ell,\end{aligned} \tag{8}$$

because this kind of integral appears in Eq. (7) after inserting the source term presented in Eq. (6). For evaluation of the integral in Eq. (8), we formally extend this representation to the multiple integrals,

$$U(\mathbf{x}, \mathbf{\Omega}, \mathbf{\Omega}_0) = \int_0^\infty \int_0^\infty \exp[-\sigma_t(\ell_1 + \ell_2)] \times \delta(\mathbf{x} - \ell_1\mathbf{\Omega} - \ell_2\mathbf{\Omega}_0)\mathrm{d}\ell_1\mathrm{d}\ell_2 = \int_{\mathbb{R}^3} \exp[-\sigma_t(\ell_1 + \ell_2)]\Theta(\ell_1)\Theta(\ell_2)\delta(\ell_3) \times \delta(\mathbf{x} - \ell_1\mathbf{\Omega} - \ell_2\mathbf{\Omega}_0 - \ell_3(\mathbf{\Omega} \times \mathbf{\Omega}_0))\mathrm{d}\ell_1\mathrm{d}\ell_2\mathrm{d}\ell_3. \tag{9}$$

Furthermore, we perform a variable transformation $\mathbf{u} : \mathbb{R}^3 \to \mathbb{R}^3$ according to

$$\mathbf{u}(\ell_1, \ell_2, \ell_3) = \ell_1\mathbf{\Omega} + \ell_2\mathbf{\Omega}_0 + \ell_3(\mathbf{\Omega} \times \mathbf{\Omega}_0). \tag{10}$$

The corresponding Jacobian determinant belonging to this transformation is given by

$$\frac{\partial(u_1, u_2, u_3)}{\partial(\ell_1, \ell_2, \ell_3)} = \det(\mathbf{\Omega}, \mathbf{\Omega}_0, \mathbf{\Omega} \times \mathbf{\Omega}_0) = \| \mathbf{\Omega} \times \mathbf{\Omega}_0\|^2, \tag{11}$$

which is, apart from the case $\mathbf{\Omega} = \mathbf{\Omega}_0$, always nonzero so that Eq. (10) represents a bijective map. The situation when both directions are equal will be considered below. Regarding the inverse of Eq. (10), we have

$$\boldsymbol{\ell} = \boldsymbol{\ell}(u_1, u_2, u_3) = \frac{1}{\| \mathbf{\Omega} \times \mathbf{\Omega}_0\|^2} \begin{pmatrix} [\mathbf{\Omega} - (\mathbf{\Omega} \cdot \mathbf{\Omega}_0)\mathbf{\Omega}_0] \cdot \mathbf{u} \\ [\mathbf{\Omega}_0 - (\mathbf{\Omega} \cdot \mathbf{\Omega}_0)\mathbf{\Omega}] \cdot \mathbf{u} \\ (\mathbf{\Omega} \times \mathbf{\Omega}_0) \cdot \mathbf{u} \end{pmatrix}. \tag{12}$$

By using the substitution rule for multiple integrals we obtain the representation

$$U(\mathbf{x}, \mathbf{\Omega}, \mathbf{\Omega}_0) = \int_{\mathbb{R}^3} \exp[-\sigma_t(\ell_1(\mathbf{u}) + \ell_2(\mathbf{u}))] \times \Theta(\ell_1(\mathbf{u}))\Theta(\ell_2(\mathbf{u}))\delta(\ell_3(\mathbf{u})) \frac{\delta(\mathbf{x} - \mathbf{u})}{\| \mathbf{\Omega} \times \mathbf{\Omega}_0\|^2}\mathrm{d}\mathbf{u} = \exp[-\sigma_t(\ell_1(\mathbf{x}) + \ell_2(\mathbf{x}))] \times \Theta(\ell_1(\mathbf{x}))\Theta(\ell_2(\mathbf{x}))\delta(\det(\mathbf{x}, \mathbf{\Omega}, \mathbf{\Omega}_0)). \tag{13}$$

In the special case of $\mathbf{\Omega} = \mathbf{\Omega}_0$, the first integral representation of Eq. (9) can be directly evaluated in polar coordinates, yielding

$$U(\mathbf{x}, \mathbf{\Omega}_0, \mathbf{\Omega}_0) = \int_0^{\pi/2} \int_0^\infty \exp[-\sigma_t\xi\sqrt{2}\sin(\vartheta + \pi/4)] \times \delta(\mathbf{x} - \xi\sqrt{2}\sin(\vartheta + \pi/4)\mathbf{\Omega})\xi\mathrm{d}\xi\mathrm{d}\vartheta = \frac{\exp(-\sigma_t \| \mathbf{x} \|)}{2 \| \mathbf{x} \|}\delta\left(\frac{\mathbf{x}}{\| \mathbf{x} \|} - \mathbf{\Omega}\right) \times \int_0^{\pi/2} \frac{\mathrm{d}\vartheta}{\sin^2(\vartheta + \pi/4)} = \frac{\exp(-\sigma_t \| \mathbf{x} \|)}{\| \mathbf{x} \|}\delta\left(\frac{\mathbf{x}}{\| \mathbf{x} \|} - \mathbf{\Omega}\right). \tag{14}$$

Regarding Eq. (13), the argument of the δ function shows that U is nonzero if $\dim(\mathrm{Lin}(\boldsymbol{x}, \mathbf{\Omega}, \mathbf{\Omega}_0)) < 3$. As an example, in the special case of $\mathbf{\Omega}_0 = \hat{\boldsymbol{z}}$, the corresponding normal vector is $\mathbf{\Omega} \times \hat{\boldsymbol{z}} = (\sin\theta\sin\phi, -\sin\theta\cos\phi, 0)^T$ and $\delta(\mathbf{x} \cdot (\mathbf{\Omega} \times \hat{\boldsymbol{z}}) = \delta(\phi_\rho - \phi)/(\rho\sin\theta)$, where $\rho = \sqrt{x^2 + y^2}$ and $\tan\phi_\rho = y/x$. The resulting expression for U can then be summarized as

$$U(\mathbf{x}, \mathbf{\Omega}, \hat{\boldsymbol{z}}) = \exp(-\sigma_t\rho\tan(\theta/2)) \times \exp(-\sigma_t z)\Theta(z - \rho\cot\theta)\frac{\delta(\phi_\rho - \phi)}{\rho\sin\theta}. \tag{15}$$

Based on the previous calculation step, we find the particular solution of Eq. (5) in the form

$$G_1(\mathbf{x}, \mathbf{\Omega}) = \sigma_s f(\mathbf{\Omega} \cdot \mathbf{\Omega}_0)U(\mathbf{x} - \mathbf{x}_0, \mathbf{\Omega}, \mathbf{\Omega}_0) + \sigma_s R(-\mu_0) \times \Theta(-\mu_0) f(\mathbf{\Omega} \cdot \mathbf{\Omega}'_0)U(\mathbf{x} + \mathbf{x}_0, \mathbf{\Omega}, \mathbf{\Omega}'_0), \tag{16}$$

where U is given explicitly in Eq. (13) together with $\boldsymbol{\ell}(\mathbf{x})$ from Eq. (12). To proceed further, we need the general solution to the homogeneous transport equation

$$\mathbf{\Omega} \cdot \nabla I(\mathbf{x}, \mathbf{\Omega}) + \sigma_t(\mathbf{x})I(\mathbf{x}, \mathbf{\Omega}) = 0. \tag{17}$$

For this task, the method of characteristics is used to reduce this equation to an ordinary differential equation (ODE). Let $\mathbf{x}(s) = (x(s), y(s), z(s))^T$ be a curve in $\mathbb{R}^3$ and $\hat{I}(s, \mathbf{\Omega}) := I(\mathbf{x}(s), \mathbf{\Omega})$ and $\hat{\sigma}_t(s) := \sigma_t(\mathbf{x}(s))$ the radiance and the attenuation coefficient as function of the curve parameter s, respectively. Then, by applying the chain rule, we find the derivative

$$\frac{d\hat{I}}{ds} = \frac{\partial I}{\partial x}\frac{dx}{ds} + \frac{\partial I}{\partial y}\frac{dy}{ds} + \frac{\partial I}{\partial z}\frac{dz}{ds}. \tag{18}$$

The homogenous Eq. (17) divided through $\cos\theta$ is

$$\tan\theta\cos\phi\frac{\partial I}{\partial x} + \tan\theta\sin\phi\frac{\partial I}{\partial y} + \frac{\partial I}{\partial z} = -\frac{\sigma_t}{\cos\theta}I. \tag{19}$$

Comparing the right-hand side of Eq. (18) with the left-hand side of Eq. (19) leads to the ODEs

$$\frac{dx}{ds} = \tan\theta\cos\phi \quad \Rightarrow \quad x(s) = s\tan\theta\cos\phi + x_0,$$

$$\frac{dy}{ds} = \tan\theta\sin\phi \quad \Rightarrow \quad y(s) = s\tan\theta\sin\phi + y_0,$$

$$\frac{dz}{ds} = 1 \quad \Rightarrow \quad z(s) = s + z_0,$$

where $(x_0, y_0, z_0) \in \mathbb{R}^3$ is an arbitrary point. In the present case, we set $z_0 = 0$ to match the curve parameter s with the z coordinate. Furthermore, we take into account the boundary data $I|_{\partial V} = C(x, y, \mathbf{\Omega})$, with C being an arbitrary function depending on four variables. As a result, Eq. (17) is reduced to the ODE

$$\cos\theta\frac{\partial\hat{I}(s, \mathbf{\Omega})}{\partial s} + \hat{\sigma}_t(s)\hat{I}(s, \mathbf{\Omega}) = 0, \tag{20}$$

which is subject to $\hat{I}(0, \mathbf{\Omega}) = I(\mathbf{x}(0), \mathbf{\Omega}) = C(x_0, y_0, \mathbf{\Omega})$. The separation of variables leads to the radiance in parameter form

$$\begin{aligned}\hat{I}(s, \mathbf{\Omega}) &= C(x_0, y_0, \mathbf{\Omega}) \exp\left(-\frac{1}{\cos\theta}\int_0^s \hat{\sigma}_t(\alpha)\mathrm{d}\alpha\right)\\ &= C(x_0, y_0, \mathbf{\Omega}) \exp\left(-\frac{1}{\cos\theta}\int_0^s \sigma_t(x_0\right.\\ &\quad \left.+ \alpha\tan\theta\cos\phi, y_0 + \alpha\tan\theta\sin\phi, \alpha)\mathrm{d}\alpha\right).\end{aligned} \tag{21}$$

To obtain the result in the original coordinates, we have to perform the exchange $x_0 = x - z\tan\theta\cos\phi$, $y_0 = y - z\tan\theta\sin\phi$, and $s = z$. After that, the general solution to Eq. (17) is found to be

$$\begin{aligned}I(\mathbf{x}, \mathbf{\Omega}) &= C(x - z\tan\theta\cos\phi, y - z\tan\theta\sin\phi, \mathbf{\Omega})\\ &\quad\times \exp\left(-\frac{1}{\cos\theta}\int_0^z \sigma_t[x + (\alpha - z)\tan\theta\cos\phi,\right.\\ &\quad \left. y + (\alpha - z)\tan\theta\sin\phi, \alpha]d\alpha\right)\\ &= C(x - z\tan\theta\cos\phi, y - z\tan\theta\sin\phi, \mathbf{\Omega})\\ &\quad\times \exp\left(-\int_0^{z/\mu}\sigma_t(\mathbf{x} - \ell\mathbf{\Omega})\mathrm{d}\ell\right).\end{aligned} \tag{22}$$

In the case of the $\sigma_t \equiv$ constant, we have $I(\mathbf{x}, \mathbf{\Omega}) = C(x - z\tan\theta\cos\phi, y - z\tan\theta\sin\phi, \mathbf{\Omega})\exp(-\sigma_t z/\cos\theta)$. Next, we have to use this result for the $\sigma_t \equiv$ constant in combination with the particular solution to Eq. (16) to satisfy the angular-dependent BC. Moreover, in the case of a semi-infinite medium, we have to ensure that I_1 remains finite for all directions $\mathbf{\Omega}$, yielding $C(\cdot, \cdot, \mathbf{\Omega}) = 0$ for $\mu < 0$. Inserting the radiance in parts of the homogeneous and particular contribution into the BC of Eq. (3) results in

$$\begin{aligned}I(\mathbf{x}, \mu, \phi) + G_1(\mathbf{x}, \mu, \phi) &= R(\mu)[I(\mathbf{x}, -\mu, \phi)\\ &\quad + G_1(\mathbf{x}, -\mu, \phi)], \quad (\mathbf{x}, \mu) \in \partial V \times (0, 1].\end{aligned} \tag{23}$$

Using $I|_{\partial V} = C(x, y, \mathbf{\Omega})$ for $\mu > 0$ and $I|_{\partial V} = 0$ if $\mu < 0$ leads to

$$\begin{aligned}&C(x, y, \mathbf{\Omega}) + G_1(x, y, 0, \mu, \phi) = R(\mu)G_1(x, y, 0, -\mu, \phi)\\ &\Leftrightarrow C(x, y, \mathbf{\Omega}) = R(\mu)G_1(x, y, 0, -\mu, \phi) - G_1(x, y, 0, \mu, \phi)\end{aligned} \tag{24}$$

for $\mu > 0$. The desired single-scattered radiance within the half-space $\overline{V}$ becomes in final form

$$\begin{aligned}I_1(\mathbf{x}, \mathbf{\Omega}) &= G_1(\mathbf{x}, \mathbf{\Omega}) + [R(\mu)G_1(x - z\tan\theta\cos\phi,\\ &\quad y - z\tan\theta\sin\phi, 0, -\mu, \phi) - G_1(x - z\tan\theta\cos\phi,\\ &\quad y - z\tan\theta\sin\phi, 0, \mu, \phi)]\exp(-\sigma_t z/\mu)\Theta(\mu),\end{aligned} \tag{25}$$

with G_1 being the particular solution given in Eq. (16). We additionally want to provide the single-scattered radiance due to an isotropically emitting δ source located inside the semi-infinite medium. The corresponding solution can be directly obtained from the radiance I_1 derived above via integration according to $1/(4\pi)\int(\cdot)\mathrm{d}\mathbf{\Omega}_0$. Using the same notation as above, we find for the radiance

$$\begin{aligned}I_1(\mathbf{x}, \mathbf{\Omega}) &= F_1(\mathbf{x}, \mathbf{\Omega}) + [R(\mu)F_1(x - z\tan\theta\cos\phi,\\ &\quad y - z\tan\theta\sin\phi, 0, -\mu, \phi) - F_1(x - z\tan\theta\cos\phi,\\ &\quad y - z\tan\theta\sin\phi, 0, \mu, \phi)]\exp(-\sigma_t z/\mu)\Theta(\mu),\end{aligned} \tag{26}$$

with the particular solution F_1 that is now defined as

$$\begin{aligned}F_1(\mathbf{x}, \mathbf{\Omega}) &= \frac{\sigma_s}{4\pi}\int_0^\infty \exp(-\sigma_t\ell)\frac{\exp(-\sigma_t \parallel \mathbf{d}_1(\ell) \parallel)}{\parallel \mathbf{d}_1(\ell)\parallel^2} f(\hat{\boldsymbol{d}}_1(\ell)\cdot\mathbf{\Omega})\mathrm{d}\ell\\ &\quad + \frac{\sigma_s}{4\pi}\int_0^\infty \exp(-\sigma_t\ell)\frac{\exp(-\sigma_t \parallel \mathbf{d}_2(\ell) \parallel)}{\parallel \mathbf{d}_2(\ell)\parallel^2}\\ &\quad\times f(\hat{\boldsymbol{d}}_2(\ell)\cdot\mathbf{\Omega})R\left(\frac{z + z_0 - \ell\mu}{\parallel \mathbf{d}_2(\ell) \parallel}\right)\mathrm{d}\ell,\end{aligned} \tag{27}$$

where $\mathbf{d}_1(\ell) = \mathbf{x} - \mathbf{x}_0 - \ell\mathbf{\Omega}$, $\mathbf{d}_2(\ell) = \mathbf{x} + \mathbf{x}_0 - \ell\mathbf{\Omega}$, and $\hat{\boldsymbol{d}}_i(\ell) := \mathbf{d}_i(\ell)/\parallel \mathbf{d}_i(\ell) \parallel$ for $i = 1, 2$.

3. VERIFICATION OF THE DERIVED SOLUTIONS

In this section, the derived solutions are illustrated and verified by comparisons with the Monte Carlo method. Within the comparisons outlined below, the absorption coefficient and the reduced scattering coefficient are, respectively, assumed to be $\sigma_a = 0.01\ \mathrm{mm}^{-1}$ and $\sigma_s' = 0.6\ \mathrm{mm}^{-1}$. We furthermore consider the Henyey–Greenstein phase function for modeling the

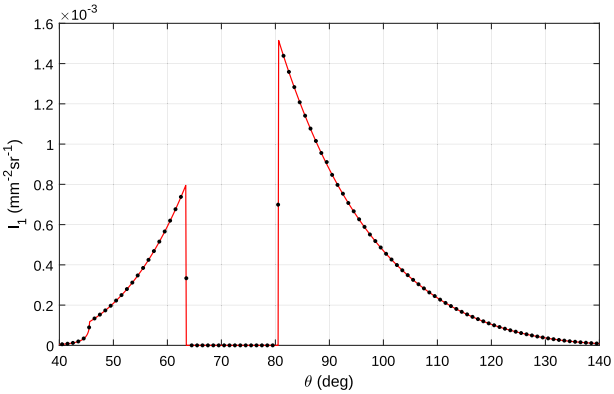

Fig. 2. Single-scattered radiance in the semi-infinite medium caused by a unidirectional point source with direction $\mathbf{\Omega}_0 = \hat{\mathbf{z}}$. The anisotropy factor for the Henyey–Greenstein phase function is set to $g = 0.3$.

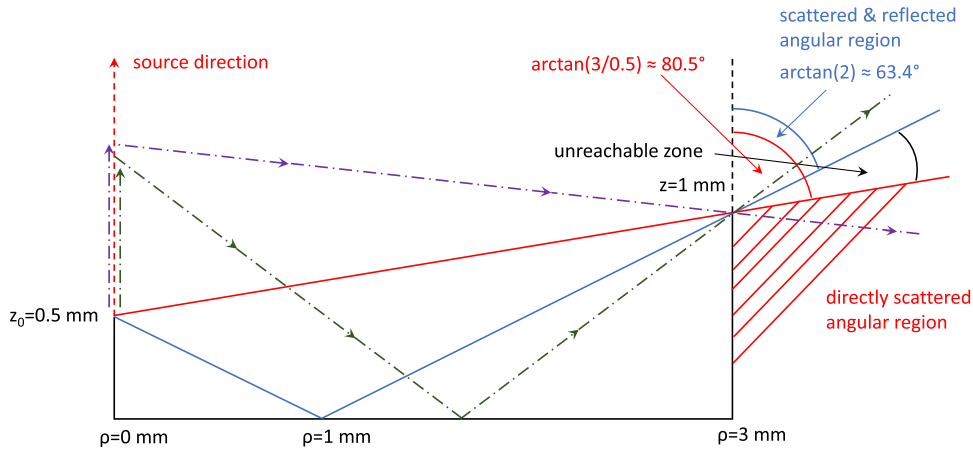

Fig. 3. Illustration of the different angular regions concerning the second numerical experiment, including two possible paths indicated by the dashed-dotted lines (green and violet).

effect of anisotropic scattering. Within the first three numerical experiments, the point of detection and the source position are set to ($\rho = 3$ mm, $z = 1$ mm) and $z_0 = 0.5$ mm, respectively, and the relative refractive index is set to $n = 1.4$. The Monte Carlo method also takes into account only one scattering event.

Figure 2 displays the single-scattered radiance within a semi-infinite medium for the case of a unidirectional point source radiating along the direction $\mathbf{\Omega}_0 = \hat{\boldsymbol{z}}$. In this case, the analytical solution for the radiance contains a Dirac function in view of the azimuthal angle. For the comparison with the Monte Carlo method, the radiance is integrated with respect to the quantity $\chi := |\phi - \phi_\rho|$. In Fig. 2, the solid line corresponds with the analytical solution given by Eq. (25), whereas the filled dots are the data predicted by the Monte Carlo method.

The light directly scattered from the source to the detector can only contribute to angles above $\approx 80.5°$, as shown by the red area in Fig. 3. For increasing theta values, the radiance decreases: first, due to the increasing distance traveled by the photons to the scattering location; second, due to the increasing distance traveled by the photons from the scattering location to the detector; and third, due to the fact that the probability for backward scattering is smaller than for forward or sideward scattering in the considered case of $g = 0.3$. The light that is backscattered and then reflected at the boundary can only contribute to angles below $\approx 63.4°$, as shown by the blue highlighted angular region. The cusp around 45.6° is due to the refractive index mismatch. Below this angle, no total internal reflection occurs.

In Fig. 4, we repeat the last numerical experiment for the source direction $\mathbf{\Omega}_0 = -\hat{\boldsymbol{z}}$. Thus, the point source located in the half-space radiates now in the direction of the reflecting boundary. As in the first comparison, an excellent agreement between the analytical solution and the Monte Carlo method is obtained.

The shape of the curve can be explained by looking at the individual fractions, as shown in Fig. 5. The red curve is the same as in Fig. 4. The blue curve is the radiance due to a source in the $\hat{\boldsymbol{z}}$ direction that stops at the boundary. Note that all light that hits the boundary unscattered is neglected. It is zero outside of a certain window, since it has a finite length of 0.5 mm. The light that is first reflected and afterward scattered is shown in

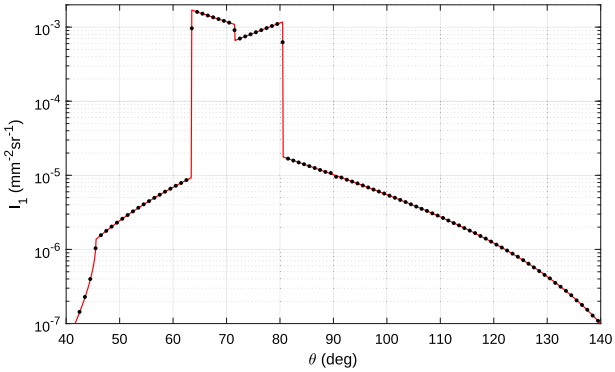

Fig. 4. Single-scattered radiance in the semi-infinite medium caused by a unidirectional point source with direction $\mathbf{\Omega}_0 = -\hat{\boldsymbol{z}}$. The anisotropy factor for the Henyey–Greenstein phase function is set to $g = 0.3$.

the green curve (extenuated source at boundary position in the $\hat{\boldsymbol{z}}$ direction); it can get to the detector directly after scattering (angles above arctan(3)) or can be reflected again (angles below arctan(3)). The sum of the two parts (blue and green) results in the red curve. The critical angle, where total internal reflection occurs, is $\arcsin(1/1.4) \approx 45.6°$.

For the next comparison, we consider the case of an isotropic point source located in the semi-infinite medium with a reflecting boundary. Figure 6 shows the angle-resolved radiance for the angular difference $\chi = 40.5°$ and the detection position ($\rho = 3$ mm, $z = 0.05$ mm). The analytical solution is denoted by the smooth curve, whereas the Monte Carlo method corresponds to the noisy line.

Figure 7 displays the same situation for the smaller angular difference $\chi = 0.5°$ and the unchanged position ($\rho = 3$ mm, $z = 0.05$ mm). As in the comparisons above, an excellent agreement between the analytical solution and the Monte Carlo method is obtained for all angles. The analytical solution is denoted by the smooth curve, whereas the Monte Carlo method corresponds to the noisy line.

For the last numerical experiment, we verify the parametrization of the curve associated with the direction vector $\mathbf{\Omega}$ of the single-scattered radiance [Eq. (16)]. From Eq. (13), we see

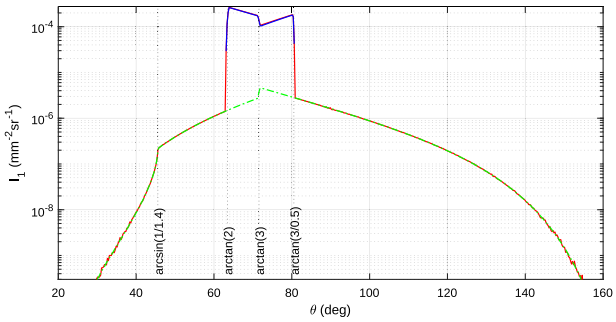

Fig. 5. Single-scattered radiance in the semi-infinite medium caused by a unidirectional point source with direction $\mathbf{\Omega}_0 = -\hat{\mathbf{z}}$.

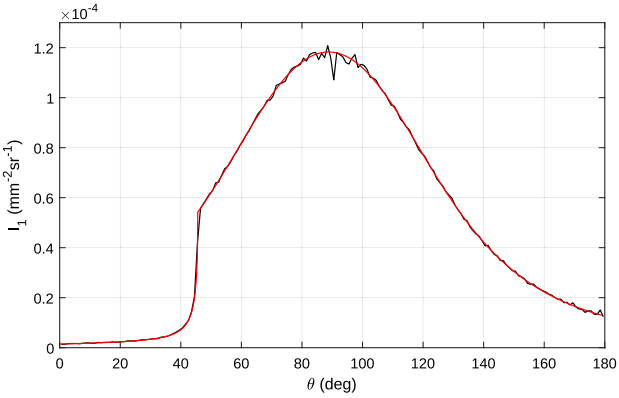

Fig. 6. Single-scattered radiance in the semi-infinite medium caused by an isotropic point source. The anisotropy factor for the Henyey–Greenstein phase function is set to $g = 0.5$.

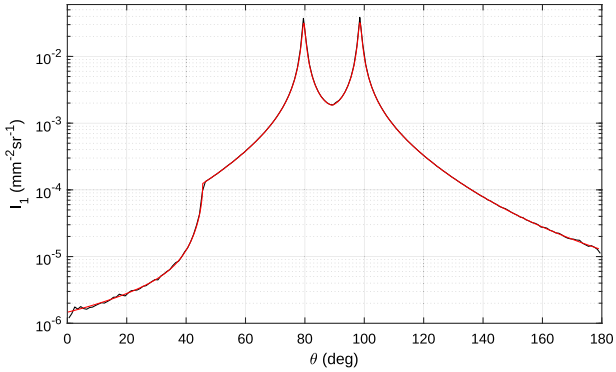

Fig. 7. Single-scattered radiance in the semi-infinite medium caused by an isotropic point source. The anisotropy factor for the Henyey–Greenstein phase function is set to $g = 0.5$.

that the radiance is only nonzero if $\det(\mathbf{x}, \mathbf{\Omega}, \mathbf{\Omega}_0) = 0$, which implies the relation $\mathbf{\Omega} \cdot (\hat{\boldsymbol{x}} \times \mathbf{\Omega}_0) = 0$ or $\mathbf{\Omega} \in \mathrm{Lin}(\hat{\boldsymbol{x}}, \mathbf{\Omega}_0)$. Furthermore, due to the step functions appearing in Eq. (13), it can be shown that $\mathbf{\Omega} \in \mathrm{Cone}(\hat{\boldsymbol{x}}, -\mathbf{\Omega}_0) = \{\alpha\hat{\boldsymbol{x}} - \beta\mathbf{\Omega}_0 | \alpha, \beta \geq 0\}$. The direction vector is normalized according to $\| \mathbf{\Omega} \| = 1$, yielding the equation $\alpha^2 + \beta^2 - 2\alpha\beta(\hat{\boldsymbol{x}} \cdot \mathbf{\Omega}_0) = 1$. This is an equation for an ellipse, which can be written in parameter form according to

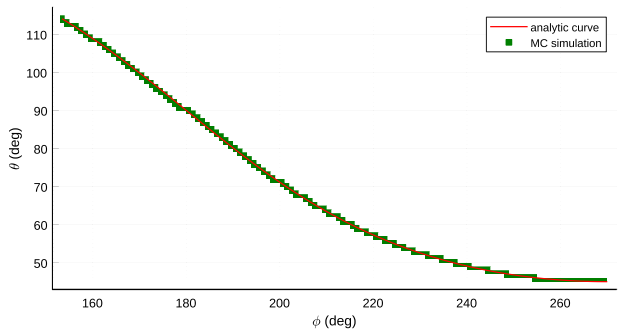

Fig. 8. Geometric location of the direction vector $\mathbf{\Omega}$ for which the single-scattered radiance in Eq. (16) is nonzero.

$$\alpha(t) = \frac{\sin(t - \vartheta)}{\sqrt{1 - (\hat{\boldsymbol{x}} \cdot \mathbf{\Omega}_0)^2}}, \qquad \beta(t) = \frac{\sin(t + \vartheta)}{\sqrt{1 - (\hat{\boldsymbol{x}} \cdot \mathbf{\Omega}_0)^2}}, \tag{28}$$

where $\vartheta := \arctan\sqrt{(1 - (\hat{\boldsymbol{x}} \cdot \mathbf{\Omega}_0))/(1 + (\hat{\boldsymbol{x}} \cdot \mathbf{\Omega}_0))}$ and $\vartheta \leq t \leq \pi - \vartheta$. Thus, for given vectors $\hat{\boldsymbol{x}}$ and $\mathbf{\Omega}_0$, the corresponding direction vector is parameterized by $\mathbf{\Omega}(t) = \alpha(t)\hat{\boldsymbol{x}} - \beta(t)\mathbf{\Omega}_0$. We note that within the above parametrization, the condition $\alpha, \beta \geq 0$ has already been considered. In Fig. 8, we compare the above parameter form with the curve predicted by the Monte Carlo method for the source position $\mathbf{x}_0 = \mathbf{0}$. Both methods lead to the same geometric location of the single-scattered radiance [Eq. (16)].

4. CONCLUDING REMARKS

In this paper, we have derived some explicit analytical solutions for the single-scattered radiance in the infinite and semi-infinite geometry containing a unidirectional beam source or an isotropic point source. The resulting analytical solutions, which are general in view of the boundary reflection function as well as the scattering phase function, have been compared to the Monte Carlo simulations showing, within the stochastic nature of the Monte Carlo simulations, an exact agreement. They can be used to perform physically based rendering as well as for verification of the Monte Carlo method. In addition, the derived expression for the single-scattered radiance is needed when seeking a similar analytical solution of the RTE in a double-scattering approximation. Moreover, the presented solution approach also can be extended to obtain solutions for the slab geometry. Further applications of the derived solutions can be found in the early diagnosis of tissue alterations. For example, most cancers have their origin in the epithelium, which is relatively easy to access by light-based measurements. When the tissue's microstructure is changed, the scattering function is altered. Using optical apparatuses, which are sensitive to changes of the scattering function such as measurements in the spatial frequency using high spatial frequencies, and applying the derived equations allows the determination of the scattering function. Thus, this might lead to an improved early diagnosis of tissue malformations. Similarly, for microscopic applications in the spatial domain, where the reflected light is detected in the small area of the incident light beam, the probability that mainly the

single scattered light is measured is high. Thus, it is also probable that the derived equations are applicable.

Disclosures. The authors declare no conflicts of interest.

REFERENCES

1. A. Ishimaru, *Wave Propagation and Scattering in Random Media* (Academic, 1978).
2. K. M. Case and P. F. Zweifel, *Linear Transport Theory* (Addison-Wesley, 1967).
3. F. Martelli, S. Del Bianco, A. Ismaelli, and G. Zaccanti, *Light Propagation through Biological Tissue and Other Diffusive Media: Theory, Solutions, and Software* (SPIE, 2010).
4. J. R. Frisvad, T. Hachisuka, and T. K. Kjeldsen, "Directional dipole model for subsurface scattering," ACM Trans. Graph. **34**, 5 (2014).
5. R. Habel, P. Christensen, and W. Jarosz, "Photon beam diffusion: a hybrid Monte Carlo method for subsurface scattering," Comput. Graph. Forum **32**, 27–37 (2013).
6. R. Ramamoorthi and P. Hanrahan, "A signal-processing framework for inverse rendering," in *Proceedings of SIGGRAPH* (2001), pp. 117–128.
7. W. Jakob, E. d'Eon, O. Jakob, and S. Marschner, "A comprehensive framework for rendering layered materials," in *Proceedings of SIGGRAPH* (2014), pp. 1–14.
8. H. W. Jensen and P. H. Christensen, "Efficient simulation of light transport in scenes with participating media using photon maps," in *Proceedings of SIGGRAPH* (2002), pp. 311–320.
9. E. d'Eon and G. Irving, "A quantized-diffusion model for rendering translucent materials," ACM Trans. Graph. **30**, 56 (2011).
10. M. I. Mishchenko, L. D. Travis, and A. A. Lacis, *Multiple Scattering of Light by Particles* (Cambridge University, 2006).
11. D. A. Boas, C. Pitris, and P. F. Ramanujam, *Handbook of Biomedical Optics* (CRC, 2012).
12. L. Wang, S. L. Jacques, and L. Zheng, "MCML–Monte Carlo modeling of light transport in multi-layered tissues," Comput. Methods Programs Biomed. **47**, 131–146 (1995).
13. F. Long, F. Li, X. Intes, and S. P. Kotha, "Radiative transfer equation modeling by streamline diffusion modified continuous Galerkin method," J. Biomed. Opt. **21**, 036003 (2016).
14. H. Fujii, Y. Yamada, G. Chiba, Y. Hoshi, K. Kobayashi, and M. Watanabe, "Accurate and efficient computation of the 3D radiative transfer equation in highly forward-peaked scattering media using a renormalization approach," J. Comput. Phys. **374**, 591–604 (2018).
15. F. Asllanaj, S. Contassot-Vivier, A. Liemert, and A. Kienle, "Radiative transfer equation for predicting light propagation in biological media: comparison of a modified finite volume method, the Monte Carlo technique, and an exact analytical solution," J. Biomed. Opt. **19**, 015002 (2014).
16. V. A. Markel, "Modified spherical harmonics method for solving the radiative transport equation," Waves Random Complex Media **14**, L13–L19 (2004).
17. A. Liemert and A. Kienle, "Green's function of the time-dependent radiative transport equation in terms of rotated spherical harmonics," Phys. Rev. E **86**, 036603 (2012).
18. M. Machida, G. Y. Panasyuk, J. C. Schotland, and V. A. Markel, "The Green's function for the radiative transport equation in the slab geometry," J. Phys. A **43**, 065402 (2010).
19. M. Machida, "Singular eigenfunctions for the three-dimensional radiative transport equation," J. Opt. Soc. Am. A **31**, 67–74 (2014).
20. A. Liemert and A. Kienle, "Explicit solutions of the radiative transport equation in the P_3 approximation," Med. Phys. **41**, 111916 (2014).
21. T. Spott and L. O. Svaasand, "Collimated light sources in the diffusion approximation," Appl. Opt. **39**, 6453–6465 (2000).
22. S. A. Carp, S. A. Prahl, and V. Venugopalan, "Radiative transport in the delta-P1 approximation: accuracy of fluence rate and optical penetration depth predictions in turbid semi-infinite media," J. Biomed. Opt. **9**, 632–648 (2004).
23. I. Seo, C. K. Hayakawa, and V. Venugopalan, "Radiative transport in the delta-approximation for semi-infinite turbid media," Med. Phys. **35**, 681–693 (2008).
24. M. L. Shendeleva, "Single-scattering solutions to radiative transfer in infinite turbid media," J. Opt. Soc. Am. A **30**, 2169–2174 (2013).
25. M. L. Shendeleva, "Time-domain solution to the radiative transfer equation in an infinite turbid medium with linearly anisotropic scattering," J. Opt. Soc. Am. A **32**, 471–477 (2015).
26. B. Sun, R. Ramamoorthi, S. G. Narasimhan, and S. K. Nayar, "A practical analytic single scattering model for real time rendering," ACM Trans. Graph. **24**, 1040–1049 (2005).
27. V. Pegoraro, M. Schott, and S. G. Parker, "A closed-form solution to single scattering for general phase functions and light distributions," Comput. Graph. Forum **29**, 1365–1374 (2010).